JPET Fast Forward. Published on July 3, 2019 as DOI: 10.1124/jpet.119.258343
This article has not been copyedited and formatted. The final version may differ from this version.

Liraglutide attenuates pre-established atherosclerosis in apolipoprotein E deficient mice *via* regulation of immune cell phenotypes and pro-inflammatory mediators

Robyn Bruen[1], Seán Curley[2] Sarina Kajani[2], Gina Lynch[3], Marcella E. O'Reilly[3], Eugène T. Dillon[4], Eoin P. Brennan[2], Mary Barry[5], Stephen Sheehan[5] Fiona C. McGillicuddy[2] and Orina Belton[1*].

Diabetes Complications Research Centre, [1]School of Biomolecular and Biomedical Science, [2]School of Medicine, UCD Conway Institute, University College Dublin, Belfield, Dublin 4, Ireland.

[3]School of Public Health, Physiotherapy and Sports Science, University College Dublin, Belfield, Dublin 4, Ireland.

[4]Mass Spectrometry Resource, UCD Conway Institute, University College Dublin, Belfield, Dublin 4, Ireland.

[5]Vascular Surgery, St. Vincent's University Hospital, Dublin 4, Ireland.

Running title: Reduced inflammation in atherosclerosis regression

*Correspondence: Orina Belton, Diabetes Complications Research Centre, School of Biomolecular and Biomedical Science, UCD Conway Institute, University College Dublin, Belfield, Dublin 4, Ireland.

Tel: +353 1 7166748

Fax: +353 1 716 6701

Email: orina.belton@ucd.ie

Non-standard Abbreviations

ANOVA: analysis of variance; ApoE$^{-/-}$: apolipoprotein E knockout; BMDM: bone marrow-derived macrophage; Cat: cathepsin; CCR2: CC Chemokine receptor 2; Ct: cycle threshold; CVD: cardiovascular disease; DC: dendritic cell; DP: diseased plaque; DPP-4; dipeptidyl peptidase-4; DTT: dithiothreitol; ELISA: enzyme-linked immunosorbent assay; FBS: fetal bovine serum; GLP-1: glucagon-like peptide-1; GLP-1RA: GLP-1 receptor agonist; HFHCD: high-fat high-cholesterol diet; IAA: iodoacetemide; IFN-γ: interferon-gamma; IL: interleukin; iNOS: inducible nitric oxide synthase; IPA: ingenuity pathway analysis; LEADER trial: Liraglutide Effect and Action in Diabetes: Evaluation of Cardiovascular Outcomes Results trial; LFD: low-fat diet; LFQ: label-free quantification; Lir: liraglutide; LN: lymph node; LPS: lipopolysaccharide; MCP-1: monocyte chemoattractant protein-1; M-CSF: macrophage-colony stimulating factor; PBMC: peripheral blood mononuclear cell; PBS: phosphate buffered saline; P-S: penicillin-streptomycin; qRT-PCR: quantitative real-time PCR; RDF: relatively disease free; RPMI: Roswell Park Memorial Institute; sc: subcutaneous; TNF-α: tumour necrosis factor-alpha; VC: vehicle control.

JPET Fast Forward. Published on July 3, 2019 as DOI: 10.1124/jpet.119.258343
This article has not been copyedited and formatted. The final version may differ from this version.

Number of text pages: 24

Number of tables: 2

Number of figures: 6

Number of references: 31

Number of words in the abstract: 246

Number of words in the significance statement: 70 words

Number of words in the introduction: 659

Number of words in the discussion: 1,377

Keywords: Atherosclerosis, ApoE$^{-/-}$ mice, GLP-1 receptor agonists, Inflammation, Liraglutide, Macrophages

Abstract

Recently we have shown the glucagon-like peptide-1 receptor agonist (GLP-1RA), liraglutide (Lir), inhibits early atherosclerosis development *in vivo* by modulating immune cell function. We hypothesized Lir could attenuate pre-established disease by modulating monocyte/macrophage phenotype to induce athero-protective responses. Human atherosclerotic plaques obtained post-endarterectomy and human peripheral blood macrophages were treated *ex vivo* with Lir. In parallel, apolipoprotein E deficient ($ApoE^{-/-}$) mice received a high-fat, high-cholesterol diet to induce atherosclerosis for 8 weeks, after which $ApoE^{-/-}$ mice received 300μg/kg Lir daily or vehicle control, for a further 4 weeks to investigate attenuation of atherosclerosis. Lir inhibited pro-inflammatory monocyte chemoattractant protein-1 (MCP-1) secretion from human endarterectomy samples and, MCP-1, tumour necrosis factor-alpha (TNF-α) and interleukin-1beta secretion from human macrophages following *ex vivo* treatment. An increase in CD206 mRNA and IL-10 secretion was also detected which imply resolution of inflammation. Importantly, Lir significantly attenuated pre-established atherosclerosis in $ApoE^{-/-}$ mice in the whole aorta and aortic root. Proteomic analysis of $ApoE^{-/-}$ bone marrow cells showed Lir up-regulated the pro-inflammatory cathepsin protein family, which was abolished in differentiated macrophages. In addition, flow cytometry analysis of bone marrow cells induced a shift towards reduced pro-inflammatory and increased anti-inflammatory macrophages. Lir attenuates pre-established atherosclerosis *in vivo via* altering pro-inflammatory mediators. This is the first study to describe a mechanism through which Lir attenuates atherosclerosis by increasing bone marrow pro-inflammatory protein expression, which is lost in differentiated bone marrow-derived macrophages. This contributes to our understanding of the anti-inflammatory and cardio-protective role of GLP-1RAs.

Significance Statement:

It is critical to understand the mechanisms through which liraglutide (Lir) mediates a cardio-protective effect as many type 2 diabetic medications increase the risk of myocardial infarction and stroke. We have identified that Lir reduces pro-inflammatory immune cell populations and mediators from plaque-burdened murine aortas *in vivo* and augments pro-resolving bone marrow-derived macrophages in attenuation of atherosclerotic disease, which provides further insight into the athero-protective effect of Lir.

Introduction:

Atherosclerosis is a chronic progressive disease that is characterized by accumulation and deposition of lipids and fibrous elements coupled with an inflammatory response resulting in the development of an arterial atherosclerotic lesion (Ross, 1993). The earliest clinical hallmark of a developing lesion is the accumulation of lipid-laden macrophages known as foam cells which aggregate to form the 'fatty streak' (Gerhard and Duell, 1999). Fatty streaks are precursors for advanced lesions, where clinical events stem from lesion rupture or erosion, and acute occlusions due to thrombus formation, which clinically present as a myocardial infraction or stroke (Lusis, 2000).

In addition to established risk factors such as hyperlipidemia and hypertension, it is now accepted that diabetes mellitus-associated hyperglycemia and oxidative stress contribute to accelerated-atherosclerosis by modulating monocyte and macrophage function (Bornfeldt and Tabas, 2011). Work over the past decade has identified the importance of monocyte and macrophage cells in atherosclerotic plaque formation. In a simplified model, macrophages are classified as pro-inflammatory (M1) or anti-inflammatory (M2). M1 macrophages are induced by inflammatory cytokines and sustain the on-going inflammatory response *via* generation of tumour necrosis factor-alpha (TNF-α). M2 macrophages are induced by interleukin (IL)-10 and IL-4/IL-13 and promote tissue repair and healing (Fujisaka et al., 2009). M1 and M2 macrophages show plasticity in response to stimuli from the microenvironment and have functional roles in other disorders of chronic low-grade inflammation such as obesity and atherosclerosis (Fujisaka et al., 2009). We have previously shown there is an M2 to M1 switch during atherosclerotic plaque progression in human patients (de Gaetano et al., 2016) and it is now known that type 2 diabetes mellitus is characterized by a reduction in M2 populations which is supported by *in vivo* studies, which showed that a shift in M1:M2 ratio directly correlates to the development of insulin resistance (Ye et al., 2016). Stabilizing the

progression of cardiovascular disease (CVD) remains a major target in people with type 2 diabetes mellitus. Indeed, recently there has been increased emphasis on identifying the CVD safety and benefit of recently developed glucose-lowering agents.

Increasing evidence suggests that glucagon-like peptide-1 (GLP-1) therapies including liraglutide (Lir), a GLP-1 receptor agonist (GLP-1RA) may simultaneously impact on the pathogenesis of both type 2 diabetes mellitus and CVD (Arakawa et al., 2010; Nagashima et al., 2011; Gaspari et al., 2011; Rizzo et al., 2015). Dipeptidyl peptidase (DPP)-4 inhibitors and GLP-1RAs, inhibit monocyte and macrophage inflammatory responses and accumulation resulting in attenuation of atherosclerotic lesion progression in apolipoprotein E knockout ($ApoE^{-/-}$) mice (Arakawa et al., 2010; Nagashima et al., 2011) and improve endothelial cell function and reduce adhesion marker expression (Gaspari et al., 2011). Lir has also been shown to modulate inflammation and reduce oxidative stress in diabetic patients (Rizzo et al., 2015). In addition GLP-1RA have been shown to decrease pro-inflammatory macrophages in obese type 2 diabetic patients (Hogan et al., 2014) and promote M2 polarization in human monocytes from healthy volunteers (Shiraishi et al., 2012).

We have previously reported that regression of pre-established atherosclerosis *in vivo* is associated with increased M2 macrophage polarization and IL-10 secretion in the murine aorta (McCarthy et al., 2013). Recently, we have shown Lir can limit the development of early atherosclerosis in $ApoE^{-/-}$ mice, by promoting a pro-resolving macrophage phenotype (Bruen et al., 2017). This implies that Lir may protect against macrovascular complications of diabetes. To date there are limited studies which have examined the effect of Lir on immune cell phenotypes in the context of regression of pre-established atherosclerosis. This is important as most patients present with established disease, where cellular and clinical plaques are evident and the therapeutic goal is to attenuate progression or induce resolution of the disease. This present study is the first to show that Lir stabilizes plaque progression and

may induce regression of pre-established atherosclerosis *in vivo*. In addition, through phenotypic and proteomic analysis of immune cell populations it provides mechanistic insight into the athero-protective effect of the GLP-1RA, Lir, in established atherosclerotic disease.

Methods:

Human Studies

Studies were approved by St Vincent's University Hospital, Dublin Ethics Committee and adhered to international guidelines and Declaration of Helsinki principles as revised in 2008. All participants provided informed written consent. Human endarterectomy samples were obtained from consenting patients of mixed sexes post-revascularization surgery and sectioned into relatively disease-free (RDF) and diseased plaque (DP) portions. Plaque portions were cultured in Roswell Park Memorial Institute (RPMI) medium, supplemented with 10% Fetal Bovine Serum (FBS), 1% L-glutamine and 100U penicillin-streptomycin (P-S) (Bio-sciences, Dublin, Ireland) as described previously (Brennan et al., 2018; Erbel et al., 2014). Plaque sections were treated *ex vivo* with 1μM Lir (Novo Nordisk, Dublin, Ireland) or phosphate buffered saline (PBS) (Bio-sciences, Dublin, Ireland) as a vehicle control (VC) for 28h. Peripheral blood mononuclear cells (PBMCs) were isolated from whole blood by layering diluted blood in PBS (1:1) onto lymphoprep and centrifuging for 25min at 400xg. The PBMC layer was removed and centrifuged for 5min at 800xg to remove platelets. Cells were resuspended in M199 medium (Analab, Dublin, Ireland), supplemented with 10% human serum (Sigma-Aldrich, Wicklow, Ireland) and 100U P-S, and plated on 10cm petri dishes for 2h. Adherent cells after 2h were considered monocytes and these cells were counted and re-seeded in 12-well plates at a density of $1x10^6$ cells/ml M199 medium containing 100ng/ml monocyte-colony stimulating factor (M-CSF) (Biolegend, London, UK). Cells were treated with 250nM Lir or PBS VC for 6h, in the presence or absence of 100ng/ml

lipopolysaccharide (LPS) (InvivoGen, Ireland) for 4h and 5mM ATP (Sigma-Aldrich, Wicklow, Ireland) for the final hr of treatments for inflammasome activation. Enzyme-linked immunosorbent assay (ELISA) was carried out on plaque and cell supernatants and quantitative real-time PCR (qRT-PCR) was performed on differentiated PBMCs.

Animals

The Animal Research and Ethics Committee, University College Dublin and the Health Products Regulatory Agency, Ireland approved all protocols which adhered to institutional and international guidelines. 8 week old C57BL/6J ApoE$^{-/-}$ male mice (C57BL/6J-ApoE^{tm1Unc}, 002052; RRID:IMSR_TAC:apoe, Charles River, Margate, UK) were housed in specific pathogen free conditions in 12h light and dark cycles. ApoE$^{-/-}$ mice were randomized to receive a high-fat (60% kcal from fat), high-cholesterol (1%) diet (HFHCD) (Research Diets Inc, New Brunswick, NJ, USA) for 8 weeks (n=10 per group) to establish disease. For analysis of established disease, 8 week old ApoE$^{-/-}$ mice were fed a low-fat (10% kcal from fat), 0% cholesterol diet (LFD) or HFHCD for a total of 12 weeks, where mice randomized to received the HFHCD received once daily Lir subcutaneous (s.c.) injections from weeks 9-12, titrated upwards for 10 days (1, 3, 10, 30, 50, 100, 150, 200, 250 and 300μg/kg) and maintained at 300μg/kg (n=21 per group) or VC PBS from weeks 9-12. Mice fed a LFD received daily PBS s.c. injections from weeks 9-12 as a control. Mice were scored daily and euthanized under isoflurane (Duggan Veterinary, Ireland) by a terminal retro-orbital bleed and cervical dislocation. Aortae, lumbar and inguinal lymph nodes (LNs), spleen, and bone marrow were harvested. The unit of analysis was a single animal or organ. Aortae were analyzed by *en face* staining (n=8 per group) or cultured *ex vivo* for 6h with aortic tissue analyzed by qRT-PCR (n=5-7 per group) and supernatants analyzed by ELISA (n=7 per group). Hearts were sectioned for aortic root analysis of atherosclerotic lesions by Oil Red O

JPET Fast Forward. Published on July 3, 2019 as DOI: 10.1124/jpet.119.258343
This article has not been copyedited and formatted. The final version may differ from this version.

staining and for F4/80^{+} macrophage cells (n=3-5 per group) as detailed in the supplemental methods. LNs, spleen and bone marrow cells were analyzed by flow cytometry (n=5 per group) and bone marrow cells were also analyzed by mass spectrometry (n=3 per group).

En face whole aorta Sudan IV and aortic root Oil Red O staining

En face staining was carried out on whole ApoE$^{-/-}$ aortae, perfused with PBS *in vivo*, fixed in 10% neutral buffered formalin, and stained using Sudan IV as in (Bruen et al., 2017). ApoE$^{-/-}$ hearts were perfused with PBS prior to freezing in OCT medium over dry ice and were stored at -80 ^{o}C until cryosectioned at -25 ^{o}C. When the aortic valves were clearly visible, eight 8µm sections per mouse were collected onto Superfrost^{TM} slides spanning a region of ~800µm. Cyrosections were dried at room temperature and frozen at -80 ^{o}C. For Oil Red O aortic root staining frozen slides were thawed at 37 ^{o}C for 1min, air-dried for 1h at room temperature and fixed with 4% paraformaldehyde for 5min, followed by 60% isopropanol for 5min. Sections were stained with Oil Red O working solution (0.5g Oil Red O in 100ml isopropanol, diluted using 3 parts stock with 2 parts deionized water, made 24h prior to staining and 0.22µm filtered) for 10min in the dark. Slides were rinsed 3 times for 2sec each with 60% isopropanol followed by a wash with dH_2O. Sections were stained with hematoxylin for 6min followed by a thorough wash for 10min using dH_2O. Slides were not dried before addition of 2-3 drops aqueous mounting medium per slide, followed by a coverslip. Coverslips were allowed to firmly adhere for 30-60min before imaging on a ScopePad550 5 Megpixel Android Microscope Camera at 4X magnification.

Bone Marrow-Derived Macrophages (BMDMs)

ApoE$^{-/-}$ BMDMs were cultured as previously described (Bruen et al., 2017). Briefly, bone marrow was flushed from femurs and tibiae for proteomics or cultured in 25% L929-

conditioned medium for 7 days. Suspension cells on day 7 of culture represented monocytes and adherent cells represented macrophages. Both monocytes and BMDMs were analyzed by flow cytometry and BMDMs by qRT-PCR.

Proteomics

Mass spectrometry analysis was carried out on bone marrow cells directly taken from femurs and tibae from $ApoE^{-/-}$ mice. Bone marrow cells were lysed in 6M urea (Sigma-Aldrich, Wicklow, Ireland) and the protein concentration was determined using a Bradford protein assay (Bio-Rad, Fannin Ltd, Dublin, Ireland) with 40µg of protein stored in 40µl of 6M urea at -20 ^{o}C. Proteins were trypsin digested with peptides, acidified and washed.

Trypsin digestion: Dithiothreitol (DTT) (Fisher Scientific, Dublin, Ireland) was used to reduce disulphide bonds of plasma protein samples followed by 30min incubation at 60 ^{o}C on a thermomixer without shaking. Samples were briefly centrifuged and 200mM iodoacetemide (IAA) (Sigma-Aldrich, Wicklow, Ireland) was added to alkylate the samples. DTT, IAA and urea concentrations were diluted using 50mM ammonium bicarbonate (Sigma-Aldrich , Wicklow, Ireland) to ensure 6mol/l urea was diluted to 2M urea before addition of trypsin. 0.5µg/µl trypsin (Sigma-Aldrich, Wicklow, Ireland) was added to each sample with a working ratio of protein to trypsin 50:1. Digestion was carried out overnight at 37 °C on a thermomixer set to 350rpm. To stop digestion, acetic acid (1% final volume) (Fisher Scientific, Dublin, Ireland) was added. Peptides were washed twice with 1% trifluoroacetic acid (Fisher Scientific, Dublin, Ireland) in deionized water using a StageTip and centrifuged at 10,000rpm for 5min. Peptides were acidified using 50% acetonitrile and 0.1% trifluoroacetic acid, then centrifuged at 10,000rpm for 5min and repeated twice. Samples were eluted using 50% acetonitrile (Fisher Scientific, Dublin, Ireland) and 0.1% trifluoroacetic acid through a StageTip. Evaporation of samples was carried out for 20-30min at 60 ^{o}C using a

CentriVap Concentrator. Samples were re-suspended in 2.5% acetonitrile and 0.5% acetic acid. Protein concentration and confirmation of peptide bonds was evaluated using the NanoDrop2000 at 218nm. Samples were centrifuged at 13,000rpm for 5min and transferred to a mass spectrometry vial.

Mass Spectrometry: Peptide samples were analyzed on a quadrupole Orbitrap (Q-Exactive, Thermo Scientific) mass spectrometer. The Orbitrap was equipped with a reversed-phase NanoLC UltiMate 3000 high performance liquid chromatograpy system (Dionex LC Packings, now Thermo Scientific, Dublin, Ireland). Peptide fractions were loaded onto C18 reversed phase columns (5cm length, 75µm inner diameter) and eluted with a linear gradient from 8 to 40% acetonitrile with 0.5% trifluoroacetic acid, in 60min at a flow rate of 3µl/min. 5µl was used as the injection volume. The Orbitrap was operated in data dependent mode, automatically switching between MS and MS2 acquisition. Survey full scan MS spectra (m/z 350-1600) were with a resolution of 70,000 and MS2 spectra with a resolution of 17,500. The twelve most intense ions were sequentially isolated and fragmented by higher-energy C-trap dissociation (O'Reilly et al., 2016).

Protein identification: Raw data from the Orbitrap was processed using MaxQuant version1.5.6.0. To identify peptides and proteins, MS/MS spectra were matched to the UniProt mouse database. Tryptic specificity allowing two missed cleavages was used for all searches. The database searches were performed with carbamidomethyl as fixed modification, and acetylation (protein N terminus) and oxidation (M) as variable modifications. Mass spectra were searched using the default setting of MaxQuant1.5.6.0, namely a false discovery rate of 1% on the peptide and protein level. Label free quantitative (LFQ) ion intensities for protein profiles were generated using signals of corresponding peptides in different nano-high performance liquid chromatograpy. MS/MS runs were matched by MaxQuant1.5.6.0 applying a mass accuracy of at least 20ppm and a maximum time window of 1min.

Proteomic data analysis: MaxQuant1.5.6.0 identified proteins and generated LFQ intensities which were analyzed using Perseus version1.4.1.3. Protein identifications were filtered to eliminate the reverse database and common contaminants. Data was filtered with stringent inclusion to obtain peptides where the peptide was present in all biological replicates in all samples. Data was log transformed and unpaired t-test comparisons of fractions were carried out. For heat map visualization, missing values were imputed with values from the normal distribution. The dataset was normalized by z-score. Proteins were analyzed for pathways using Ingenuity Pathway Analysis (IPA) (©2018 Qiagen).

Flow Cytometry analysis

Day 7 BMDMs, LNs and spleens, which were homogenized and flushed with PBS, were stained with antibodies described in Table 1. All flow cytometry antibodies were purchased from BD Biosciences, Oxford, UK (Supplemental Table 1). Flow cytometry controls included single-stains consisting of a single antibody mixed with BMDMs, LN or splenic tissue. For gating strategies, fluorescence minus one controls were used, where all antibodies excluding one, were incubated with BMDMs, LN or splenic tissue. Samples were run on the Beckman Coulter CyanADP Flow Cytometer and analyzed using FlowLogic™ software (Miltenyi Biotec Ltd, Surrey, UK).

ELISA

ELISA was performed for human TNF-α, MCP-1 and IL-1β (Thermo Fisher, Dublin, Ireland), and murine TNF-α (R&D systems, Oxon, UK) as per the manufacturer's instructions.

qRT-PCR

Cellular RNA was extracted from PBMC-derived human macrophages and ApoE$^{-/-}$ BMDMs using RNeasy Qiagen kits (Qiagen Ltd, Manchester, UK) as per the manufacturer's instructions. Murine aortas were homogenized using the Qiagen Tissue Lyser II and steel beads (Qiagen Ltd, Manchester, UK) for 10min at 30Hz, twice prior to RNA extraction, and extracted using Trizol reagent (Bio-Sciences, Dublin, Ireland). Briefly, samples were incubated on ice (5min) with addition of 1:1 chloroform:isoamyl alcohol (Sigma-Aldrich, Wicklow, Ireland), vortexed, incubated on ice (8min), centrifuged (18,500xg, 15min, 4 ^{o}C) with the aqueous layer taken, mixed with cold isopropanol (Fisher Scientific, Dublin, Ireland) and stored overnight (-20 ^{o}C). Samples were centrifuged (18,500xg, 30min) with the RNA pellet washed twice in 75% cold ethanol (Sigma-Aldrich, Wicklow, Ireland), resuspended in RNase-free water (Qiagen Ltd, Manchester, UK) and quantified using the NanoDrop2000. 100-1000ng RNA was reverse transcribed to cDNA and analyzed on a Thermo Fisher Quantstudio7 qRT-PCR machine. SYBR® Green human TNF-α (NC_000006), murine TNF-α (Y00467.1) and murine inducible nitric oxide synthase (iNOS) (NC_000017) (Table 2) (Eurofins BPT Ireland Ltd, Waterford, Ireland) sequences are available in GenBank with associated accession numbers, murine Taqman Arg-1 (Mm00475988_m1), cathepsin (Cat)B (Mm01310506_m1) and CatZ (Mm00517697_m1) were analyzed using GAPDH (human-Hs02786624_g1, murine-Mm99999915_g1) and 18S rRNA (Hs99999901_s1) (Bio-sciences, Dublin, Ireland) as reference genes. Cycle threshold (Ct) values were analyzed by the ΔΔCt method.

Statistical Analysis

All data were analyzed using GraphPad Prism 5.0c (GraphPad Software Inc, San Diego, CA, USA) and are expressed as the mean±SEM. Shapiro-Wilk normality tests were carried out to

determine if the data was parametric or non-parametric. For comparison of human endarterectomy DP PBS vs DP Lir and PBMC-derived macrophages VC+LPS vs Lir+LPS paired t-tests or Wilcoxon-matched pairs signed rank tests were used to analyze parametric or non-parametric data, respectively. For comparison of LFD vs HFHCD and HFHCD vs LFD Mann-Whitney tests were used. For multiple comparisons of animal weights a two-way analysis of variance (ANOVA) with Bonferroni's post-test was used. Statistical significance comparing DP PBS vs DP Lir, VC+LPS vs Lir+LPS and LFD vs HFHCD was considered when *$p<0.05$, **$p<0.01$ and ***$p<0.001$ and $p>0.05$ was NS and similarly considered when HFHCD vs HFHCD+Lir with $^{\$}p<0.05$, $^{\$\$}p<0.01$ and $^{\$\$\$}p<0.001$.

Results

Lir alters inflammatory chemokine secretion from human atherosclerotic plaque

Inflammatory chemokine secretion of MCP-1 from human atherosclerotic plaques cultured post-endarterectomy and treated *ex vivo* with 1μM Lir was analyzed by ELISA. Plaques were sectioned into DP and RDF portions, which served as intra-individual controls. *Ex vivo* Lir treatment significantly decreased MCP-1 secretion from human DP atherosclerotic plaques (DP VC 79.32±48.53ng/ml vs DP Lir 58.00±35.31ng/ml, n=11, $p<0.01$), whereas MCP-1 from RDF plaques was not altered compared to VC following Lir treatment (Figure 1A).

Lir modulates monocyte and macrophage phenotype

To examine if Lir can modulate monocyte/macrophage phenotype we next analyzed pro-inflammatory cytokines in human PBMC-derived macrophages. Initially MCP-1 secretion was analyzed similarly to the human endarterectomy samples, where a significant reduction in MCP-1 secretion from human PBMC-derived macrophages treated with Lir+LPS compared to the VC+LPS was detected (VC+LPS 3046±892.9ρg/ml vs Lir+LPS 2398±761.6ρg/ml,

p<0.05) (Figure 1B). Next gene expression and secretion of the pro-inflammatory cytokine, TNF-α, was analyzed in healthy PBMC-derived macrophages. There was a significant reduction in TNF-α mRNA expression in LPS-stimulated human macrophages treated with Lir compared to VC (VC+LPS 154.4±36.39 fold change vs. Lir+LPS 106.4±33.32 fold change, p<0.05) (Figure 1C), and a significant decrease in TNF-α secretion in LPS-stimulated PBMC-derived macrophages treated with Lir compared to VC (VC+LPS 804.7±201.5ρg/ml vs Lir+LPS 223.0±72.7ρg/ml, n=12, p<0.001) (Figure 1D). In addition, Lir significantly reduced IL-1β secretion following LPS stimulation (VC+LPS 72.9±17.5ρg/ml vs Lir+LPS 35.5±15.3ρg/ml, n=12, p<0.05) in PBMC-derived macrophages (Figure 1E). Thus, the effect of Lir on inhibiting MCP-1 secretion from human endarterectomy plaques and human macrophages, and TNF-α and IL-1β secretion from human macrophages suggests that Lir inhibition of pro-inflammatory cytokine secretion may alter the atherosclerotic plaque microenvironment to increase a pro-resolving or anti-inflammatory response. To investigate whether Lir could promote an anti-inflammatory response IL-10 secretion and CD206 mRNA gene expression were analyzed in human macrophages, where a trend towards increased IL-10 secretion was detected with a significant induction of CD206 mRNA in LPS-stimulated human macrophages treated with Lir (VC+LPS 1.33±0.21 fold change Lir+LPS 1.86±0.33 fold change, p<0.05) (Figure 1F-G). To comprehensively address this we employed an *in vivo* model of atherosclerosis regression.

Lir inhibits progression of established atherosclerosis in ApoE$^{-/-}$ mice despite a HFHCD challenge

Following 8 weeks HFHCD administration to establish extensive aortic lesion burden (Supplemental Figure 1), ApoE$^{-/-}$ mice were continued on HFHCDs and treated with either 300μg/kg Lir or VC for a further 4 weeks to examine the effect of Lir on established disease.

ApoE$^{-/-}$ mice fed a LFD for 12 weeks were used as controls. There were no significant differences in weight, glucose, food or water intake between HFHCD and HFHCD+Lir-treated mice at study completion (Supplemental Figure 2). Therefore all data are representative of weight-independent effects, which were anticipated given the dose of Lir used (Gaspari et al., 2013). *En face* analysis of aortae from the aortic arch to the iliac bifurcation showed HFHCD+Lir-treated ApoE$^{-/-}$ mice had a marked decrease in whole aorta atherosclerotic lesion burden (HFHCD 6.8±0.3% vs HFHCD+Lir 4.0±0.4%, $p<0.001$) and significant decrease in lesion area in all subsections of the aorta (Figure 2A-F) compared to the HFHCD-fed mice. Aortic root lesions were also quantified, where significant lesion reduction was found in the HFHCD+Lir-treated mice compared to the HFHCD-treated mice (Figure 2G-H). Simultaneously, F4/80^{+} macrophage cells were quantified in the aortic root were a reduction in macrophage content was found in HFHCD+Lir-treated ApoE$^{-/-}$ mice compared to the HFHCD control, although this result was not significant (Supplemental Figure 3). This clearly demonstrates that 4 week Lir treatment significantly attenuates established disease and may induce resolution of pre-established disease.

In parallel aortae were harvested from HFHCD- and HFHCD+Lir-treated ApoE$^{-/-}$ mice and analyzed for inflammatory cytokine secretion. Although there was a trend towards decreased TNF-α mRNA expression in HFHCD+Lir-treated aortae, Lir significantly decreased aortic TNF-α secretion (HFHCD 36.50±14.9ρg/ml vs HFHCD+Lir 2.21±2.2 ρg/ml, $p<0.001$) (Figure 3A-B). In addition, HFHCD administration induced a significant increase in mRNA expression of the M1 marker, iNOS, in ApoE$^{-/-}$ aortae, which was blunted in HFHCD+Lir-treated animals (Figure 3C). Finally, there was a trend towards increased aortic expression of the M2 marker, Arg-1, although this was not significant (Figure 3D). Together, this data suggests Lir may alter the plaque microenvironment to attenuate atherosclerosis.

JPET Fast Forward. Published on July 3, 2019 as DOI: 10.1124/jpet.119.258343
This article has not been copyedited and formatted. The final version may differ from this version.

Proteomic analysis of bone marrow cells from Lir-treated ApoE$^{-/-}$ mice highlights enrichment of pro-inflammatory pathways essential for regression

To gain insight into the mechanisms through which Lir mediates the athero-protective effect in attenuating progression of established atherosclerosis, we performed comprehensive proteomic analysis of bone marrow cells from ApoE$^{-/-}$ mice, fed a LFD for 12 week or a HFHCD for 12 weeks with either Lir or PBS daily s.c. injections for the final 4 weeks of feeding. 561 proteins were significantly altered with HFHCD+Lir (286 up-regulated and 275 down-regulated) compared to the HFHCD control. Further refinement of the data and elimination of the proteins which were significantly altered between the HFHCD and LFD groups was performed using Perseus version1.4.1.3 (Supplemental Figure 4A). This resulted in the identification of 338 and 187 significantly altered proteins in the HFHCD and HFHCD+Lir groups, respectively, compared to the LFD control. Importantly, approximately 20% of the proteins detected were unique to the HFHCD+Lir-treated group (Figure 4A). Statistical analysis using an unpaired t-test identified a unique signature of proteins associated with Lir-mediated inhibition of atherosclerosis (Figure 4B). The top 25 significantly altered proteins are listed in Supplemental Table 2. Comprehensive bioinformatic analysis using IPA was performed on proteins significantly and uniquely regulated by Lir, to elucidate potential mechanisms through which Lir mediates its effect.

Cathepsins are proteolytic macrophage enzymes documented to play a role in protein degradation and atherosclerotic lesion development. For example CatB degrades the plaque extracellular matrix and CatZ facilitates pro-inflammatory cytokine release (Zhao et al., 2016). Surprisingly, proteomic analysis identified CatB and CatZ as significantly enriched proteins in bone marrow cells from HFHCD+Lir-treated mice, despite the fact that these mice had significantly reduced lesion burden. CatB was identified in a network linked to the insulin receptor and interferon-gamma (IFN-γ), both of which are also implicated in atherosclerosis

pathogenesis (Figure 4C). Other proteins significantly up-regulated by HFHCD+Lir in this pathway are presented in Supplemental Figure 4B-E. Recently it was shown that pro-inflammatory monocytes are required for regression of atherosclerosis (Rahman et al., 2017), suggesting that enrichment of pro-inflammatory proteins in monocyte precursor cells may be associated with the inhibition of atherosclerosis observed with Lir-treated animals. Validation of the LFQ proteomic data confirmed a significant increase in bone marrow cell expression of the pro-atherogenic mediators CatB and CatZ (Figure 5A-B).

Previous studies have shown that increased pro-inflammatory monocytes are required for conversion into M2 pro-resolving macrophages in the context of atherosclerosis (Rahman et al., 2017). To identify whether this pro-inflammatory signature was maintained following monocyte to macrophage differentiation or whether macrophages adopted a pro-resolving phenotype, murine bone marrow cells were differentiated to macrophages. In contrast to what was observed in bone marrow cells, Lir significantly decreased CatB expression (HFHCD 1.0±0.07 vs HFHCD+Lir 0.8±0.06 fold change, $p<0.05$) and did not increase CatZ expression (Figure 5C-D) in macrophages. This indicates that pro-inflammatory pathways in bone marrow cells are down-regulated when undergoing differentiation to macrophages in the presence of Lir. mRNA expression of CatB and CatZ were also analyzed in LFD-, HFHCD- and HFHCD+Lir-treated $ApoE^{-/-}$ aortae. Aortic CatB and CatZ mRNA expression was significantly increased in HFHCD-fed compared to LFD- fed $ApoE^{-/-}$ mice. Interestingly, CatB mRNA expression was significantly reduced and CatZ mRNA expression was blunted in HFHCD+Lir-treated mice aortae compared to HFHCD-fed animals (Figure 5E-F). Thus it is feasible to hypothesize that Lir mediates its effect by recruiting inflammatory bone marrow cells to differentiate into pro-resolving macrophages and coincident with recent publications, this mediates regression of atherosclerosis (Rahmen et al., 2017). Therefore, the next series of

experiments were designed to investigate monocyte and macrophage populations in bone marrow and lymphoid tissues during Lir-induced attenuation of established atherosclerosis.

BMDMs from ApoE$^{-/-}$ mice are athero-protective with *in vivo* Lir treatment

ApoE$^{-/-}$ bone marrow monocytes and BMDMs were harvested from mice fed a LFD for 12 weeks, or a HFHCD for 12 weeks where the final 4 weeks mice received daily s.c. Lir or VC, were analyzed by flow cytometry for pro-inflammatory and pro-resolving phenotypes. Although there was a significant decrease in inflammatory monocytes in HFHCD-fed mice compared to LFD controls, monocytes from HFHCD+Lir-treated mice were not significantly different to those in the HFHCD control, and both HFHCD- and HFHCD+Lir-treated mice had significantly more resident monocytes compared to LFD controls (Figure 6A). The proteomic data also suggests that the inflammatory status of monocytes is increased with Lir, which is in keeping with recent studies, which show inflammatory monocytes convert to pro-resolving macrophages in athero-protection (Rahmen et al., 2017). Thus the analysis was extended to investigate the effect of Lir on macrophage populations. As expected the HFHCD-fed mice had significantly increased pro-inflammatory and decreased anti-inflammatory macrophage populations compared to the LFD control (LFD M1-like 7.3±1.1% vs. HFHCD M1-like 18.1±3.3%; LFD M2-like 92.7±1.1% vs. HFHCD M2-like 71.3±13.0%, $p<0.01$). Importantly, Lir significantly increased M2-like and decreased M1-like macrophages compared to HFHCD-treated mice (HFHCD M1-like 18.1±3.3% vs. HFHCD+Lir M1-like 5.8±1.7%; HFHCD M2-like 71.3±13.0% vs. HFHCD+Lir M2-like 94.2±1.7%, $p<0.01$). Indeed Lir normalized the M2-like macrophage populations to those comparable with LFD-treated mice (LFD M2-like 92.7±1.1% vs HFHCD+Lir M2-like 94.24±1.7%) (Figure 6B). Finally, there were similar numbers of monocyte:macrophage ratio in the bone marrow from

all animal groups (Figure 6C), suggesting Lir does not influence reduction in monocyte to macrophage number, but induces significant alterations in M2 macrophage phenotypes.

Lir alters the phenotype of lymphoid cells

Anti-inflammatory macrophages are depleted during atherosclerotic disease progression, with pro-inflammatory plaque macrophages dominating in the developing lesion (de Gaetano et al., 2016). Further flow cytometry analysis showed splenic M2 macrophages were depleted following HFHCD administration compared to LFD controls as determined by a significant inhibition of M2 phenotype (LFD M2 $4.3x10^7 \pm 2.3x10^7$ cells/mg vs. HFHCD M2 $4.7x10^6 \pm 2.5x10^6$ cells/mg, $p<0.05$). Interestingly there was no significant reduction in M2 splenic macrophages in HFHCD+Lir-treated mice compared to LFD control, suggesting Lir blocks the depletion of M2 macrophages observed in the HFHCD (Figure 6D).

Monocytes and dendritic cells (DCs) are normally recruited into advanced atherosclerotic plaques and in addition it has been shown that egress of macrophages and DCs to regional and systemic LNs occurs in regression of atherosclerosis (de Gaetano et al., 2015). Flow cytometry analysis of LNs showed a reduction of immature monocytes and DCs, and mature DCs in lymphoid tissue from HFHCD compared to LFD controls. Importantly Lir rescued mature DCs within LNs as seen by an increase in population numbers (Figure 6E), suggesting emigration of DCs from the resolving plaque. As there is a trend towards increased DC numbers in the draining LN with Lir, this data suggests that Lir may promote DC egress from atherosclerotic lesions, which is necessary for the induction of plaque regression.

Discussion

Chronic low-grade inflammation is associated with both diabetes and atherosclerosis where it has been shown that patients with type 2 diabetes mellitus and atherosclerosis have increased

pro-inflammatory monocyte and macrophage populations (Nikiforov et al., 2017). Indeed, chronic inflammatory diseases are associated with a shift in the M1:M2 ratio towards increased pro-inflammatory M1 (de Gaetano et al., 2016; Ye et al., 2016). This shift in macrophage ratio has also been linked to the development of insulin resistance in adipose tissue (Ye et al., 2016) and in the progression of atherosclerosis from an asymptomatic to symptomatic disease state (de Gaetano et al., 2015).

It was previously thought that inflammatory and resident monocytes give rise to M1 and M2 macrophages respectively (Nikforov et al., 2017; Patal et al., 2017). Fadini et al. have published that in type 2 diabetes, patients have markedly reduced anti-inflammatory monocytes through dysregulation in bone marrow function, which may have a negative impact on microangiopathy (Fadini et al. 2013). However, recent evidence has identified that inflammatory monocytes are required to induce pro-resolving macrophages to mediate regression of atherosclerosis (Rahmen et al., 2017). The monocyte-derived macrophage cells within atherosclerotic plaques are thought to originate from bone marrow cells as opposed to recruitment of new circulating monocytes (Patal et al., 2017). It has been previously shown that Lir mediates an anti-inflammatory effect in humans as observed by decreased TNF-α, IL-1β, IL-6 and C-reactive protein inhibition (Hogan et al., 2014; Shiraishi et al., 2012). Hence, this may also be of clinical importance in the context of atherosclerosis and diabetes-accelerated atherosclerosis. Recently, the Lir Effect and Action in Diabetes: Evaluation of CV Outcomes Results (LEADER) trial, reported that after 3.8 years the primary outcome of first occurrence of CVD death, non-fatal myocardial infraction or non-fatal stroke, was significantly reduced in Lir-treated patients (Marso et al., 2016).

Our previously published work provided mechanistic insight through which Lir may mediate athero-protection, where Lir dictated macrophage cell fate towards an M2 pro-resolving macrophage and halted the development of early atherosclerosis in ApoE$^{-/-}$ mice

(Bruen et al., 2017). However, as a significant portion of type 2 diabetes mellitus patients present with established atherosclerotic disease, a therapeutic goal would be to reduce and stabilize disease by blunting progression or even inducing regression of atherosclerosis whilst maintaining glycemic control. Our hypothesis was that in established atherosclerosis Lir would increase the inflammatory status of monocytes, which, when in the plaque milieu would promote a pro-resolving M2 macrophage that would dominate, reducing pro-inflammatory responses associated with disease regression and stabilization. The work presented here shows that the inflammatory microenvironment of human atherosclerotic plaques is altered in response to *ex vivo* Lir treatment, where Lir reduces secretion of MCP-1 from human endarterectomy samples. MCP-1 regulates monocyte chemotaxis and infiltration by binding to the CC chemokine receptor 2 (CCR2) (Ding et al., 2015). Both murine and human studies have shown an association with increased CCR2/MCP-1 expression and atherosclerosis progression (Ding et al., 2015). Indeed it has also been shown that increased circulating MCP-1 levels are related to increased risk of CVD and CVD mortality in patients with coronary artery disease (Ding et al., 2015). As such, strategies for inhibiting MCP-1/CCR2 are currently being explored as a therapeutic goal for the treatment of vascular disorders.

In addition, further analysis on cultured LPS-stimulated inflammatory human PBMC-macrophages showed that Lir significantly decreased secretion of the M1 pro-inflammatory mediators, MCP-1, TNF-α and IL-1β. We also showed Lir could promote anti-inflammatory responses in human macrophages by increasing IL-10 secretion and CD206 gene expression. As Lir altered the inflammatory environment of human atherosclerotic plaques, and altered the inflammatory response of macrophage phenotypes *in vitro*, we hypothesized that Lir may impact on the progression of pre-established atherosclerosis. Previous studies investigating GLP-1RAs and their effect on atherosclerosis in mice have been studied in early disease

development and progression (Bruen et al., 2017). Here, ApoE$^{-/-}$ mice were fed a HFHCD for 8 weeks to establish atherosclerotic disease and maintained on the diet for a further 4 weeks with daily s.c. Lir treatment. This is a strength of our study and is more reflective of clinical presentation of established atherosclerosis. Mice were injected with incremental doses of Lir for 10 days to minimize adverse effects and to ensure a similar dosing regimen to that used clinically in human patients. On study completion, aortae were quantified for lesion burden. Lir significantly inhibited lesion burden throughout the aortic root and whole aorta. This may be due to reduced F4/80^{+} macrophage cells, although this warrants further investigation. Therefore, this is the first report to show that Lir blocks progression of established disease and thus presents us with a unique opportunity to interrogate potential cellular mechanisms through which Lir mediates its effect on established disease.

Previous studies have shown that lixisenatide, alters the plaque milieu by decreasing macrophage content and increasing M2 macrophages in ApoE$^{-/-}$ mice (Vinué et al., 2017), although in low density lipoprotein receptor knockout mice Lir did not alter macrophage content nor aortic mRNA expression of MCP-1 or iNOS (Bisgaard et al., 2016). However, both of the aforementioned studies were performed in the context of early disease progression. Here, we analyzed the plaque microenvironment in established disease and shown that there is increased TNF-α secretion and aortic iNOS mRNA expression following a 12 week HFHCD challenge. Importantly, Lir administration inhibits aortic TNF-α secretion during attenuation of disease progression.

In atherosclerotic disease progression monocytes are recruited to the developing lesion, differentiate into macrophages, which sustain the inflammatory response and drive disease progression (Tabas and Lichtman, 2017). As bone marrow cells are recruited into lesions and are precursors for macrophage cells, we characterized these cells in the context of attenuated progression of established disease, using proteomic analysis of bone marrow cells

from ApoE$^{-/-}$ mice. Bioinformatic analysis showed an up-regulation of pro-inflammatory signalling pathways. This is in keeping with recent data which showed, that inflammatory monocyte precursor cells differentiate into anti-inflammatory macrophages during attenuation of atherosclerosis (Rahmen et al., 2017).

Cathepsin proteases are involved in destabilizing atherosclerosis and driving disease progression (Zhao et al., 2016). In bone marrow cells from HFHCD+Lir-treated mice there was an enrichment of cathepsin proteases despite reduced lesion burden in these mice. Up-regulation of this protein family suggests Lir increases the inflammatory status of bone marrow cells which are precursor cells to monocytes. To address the hypothesis, that an increased inflammatory status in bone marrow cells may convert into M2 macrophages, as previously reported in regression studies (Rahmen et al., 2017), we next investigated the pro-inflammatory cathepsin proteins in differentiated macrophages. We show that during differentiation of bone marrow monocytes from ApoE$^{-/-}$ mice treated with HFHCD+Lir the pro-inflammatory signature was lost, with no observed increase in CatB or CatZ expression. Indeed, there was a significant decrease in CatB expression in BMDMs from HFHCD+Lir mice. This data correlated with reduced CatB and CatZ mRNA expression in ApoE$^{-/-}$ mice treated with Lir, where aortic CatB expression was significantly decreased. This implies that Lir may induce a pro-inflammatory monocyte, which differentiates into a pro-resolving macrophage by down-regulating pro-inflammatory pathways in macrophages and the aorta.

Indeed, M2 macrophages have been identified in a number of murine atherosclerosis regression models (Feig et al., 2012). To address if the loss of the pro-inflammatory signal in bone marrow cells impacts on macrophage phenotype we investigated immune cell phenotypes in bone marrow, spleen and lymph nodes. The data clearly shows as expected that Lir administration increased pro-inflammatory proteins in the bone marrow of ApoE$^{-/-}$ mice, suggesting a pro-inflammatory signature and that this resulted in increased M2-like

macrophages upon differentiation. Furthermore, further flow cytometry analysis showed that the pro-resolving M2 macrophage phenotype prevails both in the bone marrow but also in splenic tissue suggesting that Lir blocks the depletion of M2 macrophages. Finally, we showed a trend towards increased numbers of migratory cells in aortic draining LNs, suggesting increased migratory ability out of lesions, and implies that this may contribute to the ability of Lir to attenuate progression and induce regression of atherosclerosis, although this warrants further investigation.

The data presented here has elucidated an important mechanism in Lir-mediated resolution of inflammation in established atherosclerosis, where pro-inflammatory bone marrow cells differentiate into pro-resolving macrophages and likely induce plaque egress of immune cells promoting repair and inhibiting lesion burden.

Acknowledgements

We would also like to acknowledge the vascular surgery staff and participating patients at St. Vincent's University Hospital (Dublin, Ireland) for providing human carotid plaque material and the UCD Conway Institute Core Facilities in particular Ms. Catherine Moss, UCD Genomics Core, Dr. Alfonso Blanco, UCD Flow Cytometry Core and Dr. Dimitri Scholz, UCD Imaging Core, Ms. Janet McCormack UCD Research Pathology Core and the UCD Proteomics Core for their technical support.

Authorship Contributions:

Participated in research design: Bruen, McGillicuddy and Belton.

Conducted experiments: Bruen, Curley, Kajani, Lynch, O'Reilly and Dillon.

Contributed human endarterectomy samples: Barry and Sheehan.

Performed data analysis: Bruen, Dillon and Brennan.

Wrote or contributed to the writing of the manuscript: Bruen and Belton.

References

Arakawa M, Mita T, Azuma K, Ebato C, Goto H, Nomiyama T, Fujitani Y, Hirose T, Kawamori R and Watada H (2010) Inhibition of monocyte adhesion to endothelial cells and attenuation of atherosclerotic lesion by a glucagon-like peptide-1 receptor agonist, exendin-4. Diabetes 59: 1030-1037.

Bisgaard LS, Bosteen MH, Fink LN, Sørensen CM, Rosendahl A, Mogensen CK, Rasmussen SE, Rolin B, Nielsen LB and Pedersen TX (2016) Liraglutide reduces both atherosclerosis and kidney inflammation in moderately uremic LDLr-/- mice. PLoS One 11(12): e0168396.

Bornfeldt KE, Tabas I (2011) Insulin resistance, hyperglycemia, and atherosclerosis. Cell Metab 14(5): 575-585.

Brennan EP, Mohan M, McClelland A, Tikellis C, Ziemann M, Kaspi A, Gray SP, Pickering R, Tan SM, Ali-Shah ST, Guiry PJ, El-Osta A, Jandeleit-Dahm K, Cooper ME, Godson C and Kantharidis P (2018) Lipoxins Regulate the Early Growth Response-1 Network and Reverse Diabetic Kidney Disease. J Am Soc Nephrol 29(5): 1437-1448.

Bruen R, Curley S, Kajani S, Crean D, O'Reilly ME, Lucitt MB, Godson CG, McGillicuddy FC and Belton O (2017) Liraglutide dictates macrophage phenotype in apolipoprotein E null mice during early atherosclerosis. Cardiovasc Diabetol 16(1): 143.

de Gaetano M, Crean D, Barry M and Belton O (2016) M1- and M2-type macrophage responses are predictive of adverse outcomes in human atherosclerosis. Front Immunol 7: 275.

de Gaetano M, Alghamdi K, Marcone S and Belton O (2015) Conjugated linoleic acid induces an atheroprotective macrophage M2 phenotype and limits foam cell formation. J Inflamm (Lond) 19: 12-15.

Ding D, Su D, Li X, Li Z, Wang Y, Qiu J, Lin P, Zhang Y, Guo P, Xia M, Li D, Yang Y, Hu G and Ling W (2015) Serum levels of monocyte chemoattractant protein-1 and all-cause and cardiovascular mortality among patients with coronary artery disease. PLoS One 18;10(3): e0120633.

Erbel C, Okuyucu D, Akhavanpoor M, Zhao L, Wangler S, Hakimi M, Doesch A, Dengler TJ, Katus HA and Gleissner CA (2014) A human *ex vivo* atherosclerotic plaque model to study lesion biology. J Vis Exp 87: 50542.

Fadini GP, de Kreutzenberg SV, Boscaro E, Albiero M, Cappellari R, Kränkel N, Landmesser U, Toniolo A, Bolego C, Cignarella A, Seeger F, Dimmeler S, Zeiher A, Agostini C and Avogaro A (2013) An Unbalanced monocyte population in peripheral blood and bone marrow of patients with type 2 diabetes has an impact on microangiopathy. Diabetologia 56(8):1856-1866.

Feig JE, Vengrenyuk Y, Reiser V, Wu C, Statnikov A, Aliferis CF, Garabedian MJ, Fisher EA and Puig O (2012) Regression of atherosclerosis is characterized by broad changes in the plaque macrophage transcriptome. PLoS One 7(6): e39790.

Fujisaka S, Usui I, Bukhari A, Ikutani M, Oya T, Kanatani Y, Tsuneyama K, Nagai Y, Takatsu K, Urakaze M, Kobayashi M and Tobe K (2009) Regulatory mechanisms for adipose tissue M1 and M2 macrophages in diet-induced obese mice. Diabetes 58(11): 2574-2582.

Gaspari T, Welungoda I, Widdop RE, Simpson RW and Dear AE (2013) The GLP-1 receptor agonist liraglutide inhibits progression of vascular disease via effects on atherogenesis, plaque stability and endothelial function in an ApoE$^{-/-}$ mouse model. Diab Vasc Dis Res 10(4):353-360.

Gaspari T, Liu H, Welungoda I, Hu Y, Widdop RE, Knudsen LB, Simpson RW and Dear AE (2011) A GLP-1 receptor agonist liraglutide inhibits endothelial cell dysfunction and vascular adhesion molecule expression in an ApoE-/- mouse model. Diab Vasc Dis Res 8(2): 117-124.

Gerhard GT and Duell PB (1999) Homocysteine and atherosclerosis. Curr Opin Lipidol 10:417-429.

Hogan AE, Goatswe G, Lynch L, Corrigan MA, Woods C, O'Connell J and O'Shea D (2014) Glucagon-like peptide 1 analogue therapy directly modulates innate immune-mediated inflammation in individuals with type 2 diabetes mellitus. Diabetologia 57(4): 781-784.

Lusis AJ (2000) Atherosclerosis. Nature 407(6801): 233-241.

Marso SP, Daniels GH, Brown-Frandsen K, Kristensen P, Mann JFE, Nauck MA, Nissen SE, Pocock S, Poulter NR, Ravn LS, Steinberg WM, Stockner M, Zinman B, Bergenstal RM and Buse JB for the LEADER Steering Committee on behalf of the LEADER Trial Investigators (2016) Liraglutide and Cardiovascular Outcomes in Type 2 Diabetes. N Engl J Med 375(4): 311-322.

McCarthy C, Duffy MM, Mooney D, James WG, Griffin MD, Fitzgerald DJ and Belton O (2013) IL-10 mediates the immunoregulatory response in conjugated linoleic acid-induced regression of atherosclerosis. Faseb J 27: 499-510.

Nagashima M, Watanabe T, Terasaki M, Tomoyasu M, Nohtomi K, Kim-Kaneyama J, Miyazaki A and Hirano T (2011) Native incretins prevent the development of atherosclerotic lesions in apolipoprotein e knockout mice. Diabetologia 54: 2649-2659.

Nikiforov NG, Galstyan KO, Nedosugova LV, Elizova NV, Kolmychkova KI and Ivanova EA (2017) Proinflammatory monocyte polarization in type 2 diabetes mellitus and coronary heart disease. Vessel Plus 1: 192-195.

O'Reilly M, Dillon E, Guo W, Finucane O, McMorrow A, Murphy A, Lyons C, Jones D, Ryan M, Gibney M, Gibney E, Brennan L, de la Llera Moya M, Reilly MP, Roche HM and McGillicuddy FC (2016) High-Density Lipoprotein Proteomic Composition, and not Efflux Capacity, Reflects Differential Modulation of Reverse Cholesterol Transport by Saturated and Monounsaturated Fat Diets. Circulation 133(19): 1838-50.

Patal AA, Zhang Y, Fullerton JN, Boelen L, Rongvaux A, Maini AA, Bigley V, Flavell RA, Gilroy DW, Asquith B, Macallan D and Yona S (2017) The fate and lifespan of human monocyte subsets in steady state and systemic inflammation. J Exp Med 214(7): 1913-1923.

Rahman K, Vengrenyuk Y, Ramsey SA, Vila NR, Girgis NM, Liu J, Gusarova V, Gromada J, Weinstock A, Moore KJ, Loke P and Fisher EA (2017) Inflammatory Ly6Chi monocytes and their conversion to M2 macrophages drive atherosclerosis regression. J Clin Invest 127(8): 2904-2915.

Rizzo M, Abate N, Chandalia M, Rizvi AA, Giglio RV, Nikolic D, Marino Gammazza A, Barbagallo I, Isenovic ER, Banach M, Montalto G, Li and Volti G (2015) Liraglutide reduces oxidative stress and restores heme oxygenase-1 and ghrelin levels in patients with type 2 diabetes: a prospective pilot study. J Clin Endocrinol Metab 100(2): 603-6.

Ross R (1993) The pathogenesis of atherosclerosis: a perspective for the 1990s. Nature 362: 801-809.

Shiraishi D, Fujiwara Y, Komohara Y, Mizuta H and Takeya M (2012) Glucagon-like peptide-1 (GLP-1) induces M2 polarization of human macrophages via STAT3 activation. Biochem Biophy Res Commun 425(2): 304-308.

Tabas I and Lichtman AH (2017) Monocyte-macrophages and T cells in atherosclerosis. Immunity 47(4): 621-634.

Vinué Á, Navarro J, Herrero-Cervera A, García-Cubas M, Andrés-Blasco I, Martínez-Hervás S, Real JT, Ascaso JF and González-Navarro H (2017) The GLP-1 analogue lixisenatide decreases atherosclerosis in insulin-resistant mice by modulating macrophage phenotype. Diabetologia 60(9): 1801-1812.

Ye L, Liang S, Guo C, Yu X, Zhao J, Zhang H and Shang W (2016) Inhibition of M1 macrophage activation in adipose tissue by berberine improves insulin resistance. Life Sci 166: 82-91.

Zhao CF and Herrington DM (2016) The function of cathepsins B, D, and X in atherosclerosis. Am J Cardiovasc Dis 6(4): 163-170.

Footnotes

Funding Statement

This work was supported by a grant from the "European Association for the Study of Diabetes (EFSD) Clinical Diabetes Research Programme in Macrovascular Complications of Diabetes" supported by AstraZeneca to Belton, McGillicuddy, Bruen and Curley and UCD-Wellcome Institutional Strategic Support Fund, jointly supported UCD and the SFI-HRB-Wellcome Biomedical Partnership to Belton.

Thesis Information

This work has been submitted in part in a PhD thesis, to University College Dublin by Robyn Bruen (March 2019).

Citation of Meeting Abstracts

Bruen R, Curley S, Kajani S, O'Reilly ME, McGillicuddy FC, Belton O. Glucagon-like peptide-1 receptor agonist, liraglutide, alters immune populations during regression of atherosclerosis. *Diabetologia.* 2018; 61(Suppl 1):S528-529.

Bruen R, Curley S, Kajani S, O'Reilly ME, Hogan A, O'Shea D, McGillicuddy FC, Belton O. Glucagon-like peptide-1 receptor agonist liraglutide impacts immune cell phenotypes in apolipoprotein E deficient mice during progression and regression of pre-established atherosclerosis. *Atherosclerosis.* 2018;275:e1-16.

Legends for Figures:

Figure 1: Pro-inflammatory mediators are reduced and anti-inflammatory mediators are increased in human atherosclerotic plaques and human PBMC-derived macrophages

A| MCP-1 secretion from RDF and DP sections of carotid (n=6) and femoral plaques (n=5) treated with 1μM Lir or VC PBS for 28h. Human PBMC-derived macrophages were treated with 250nM Lir or VC PBS for 6h with 100ng/ml LPS co-treatment for the final 4h and 5mM ATP co-treatment for the final h of treatments. mRNA was converted to cDNA and analyzed by qRT-PCR using GAPDH as a reference gene, and supernatants were analyzed by ELISA for B| MCP-1 secretion, C| TNF-α mRNA, D| TNF-α secretion, E| IL-1β secretion, F| IL-10 secretion and G| CD206 mRNA. Error bars represent A| n=11, B-C and F-G| n=7 and D-E| n=12. Shapiro-Wilk normality tests were carried out to determine if the data was parametric. Paired t-tests and Wilcoxon-matched pairs signed rank t-tests were used to compare parametric and non-parametric data, respectively, for VC vs Lir with *$p<0.05$, **$p<0.01$ and ***$p<0.001$ considered significant, while $p>0.05$ was ns.

Figure 2: Lir attenuates pre-established atherosclerosis *in vivo*

A| LFD, HFHCD or HFHCD+Lir-treated $ApoE^{-/-}$ aortae were stained by *en face* with Sudan IV for B| total, C| aortic arch, D| thoracic, E| abdominal aorta and F| iliac bifurcation, and quantified using ImageJ. G| Aortic roots were sectioned and H| quantified for atherosclerotic lesions using ImageJ. Error bars represent A-F| 8 mice (n=8 per group) and G-H| 3 mice (n=3 per group. Statistical analysis was performed carrying out Mann Whitney tests between LFD vs HFHCD where statistical significance was considered with ***$p<0.001$, **$p<0.01$ and *$p<0.05$ and HFHCD vs HFHCD+Lir where $^{\$}p<0.05$, $^{\$\$}p<0.01$ and $^{\$\$\$}p<0.001$ were considered significant.

Figure 3: Lir reduces aortic pro-inflammatory mediators

ApoE$^{-/-}$ aortae were harvested and cultured in RPMI medium, supplemented with 10% FBS and 100U P-S, for 6h with aortae and aortic supernatants from LFD-, HFHCD- and HFHCD+Lir-treated mice analyzed for A| TNF-α mRNA, B| TNF-α protein by ELISA, C| iNOS mRNA and D| Arg-1 mRNA. Error bars represent A and D| n=6, B| n=7 and C| n=5. Statistical analysis was performed carrying out Mann Whitney tests between LFD vs HFHCD where statistical significance was considered with ***$p<0.001$, **$p<0.01$ and *$p<0.05$ and HFHCD vs HFHCD+Lir where $^{\$}p<0.05$, $^{\$\$}p<0.01$ and $^{\$\$\$}p<0.001$ were considered significant.

Figure 4: Proteomic analysis of bone marrow cells during attenuation of pre-established atherosclerosis.

ApoE$^{-/-}$ bone marrow cells were analyzed by mass spectrometry. A| Number of proteins significantly regulated in the treatment groups were identified using Perseus version1.4.1.3, B| proteomic signature heat map of HFHCD vs. HFHCD+Lir bone marrow cells with red and green bars indicating proteins significantly up- or down-regulated, respectively, n=3 per group and C| identification of regulated network enriched with expression of CatB protein using IPA analysis.

JPET Fast Forward. Published on July 3, 2019 as DOI: 10.1124/jpet.119.258343
This article has not been copyedited and formatted. The final version may differ from this version.

Figure 5: Increased Cat protein expression in bone marrow cells is reversed following differentiation to macrophages and in ApoE$^{-/-}$ aortae

LFQ protein expression of A| CatB and B| CatZ from Perseus version1.4.1.3 analysis. mRNA expression of C| BMDM CatB, D| BMDM CatZ and E| aortic CatB and F| aortic CatZ from LFD, HFHCD and HFHCD+Lir-treated ApoE$^{-/-}$ mice were analyzed by qRT-PCR using GAPDH and 18S rRNA as reference genes. Error bars are representative of A-B| n=3, C-D| n=5 and E-F| n=8. Statistical analysis was performed carrying out Mann Whitney tests between LFD vs HFHCD where statistical significance was considered with *$p<0.05$, **$p<0.01$ and ***$p<0.001$ and HFHCD vs HFHCD+Lir where $^{\$}p<0.05$, $^{\$\$}p<0.01$ and $^{\$\$\$}p<0.01$ was considered significant.

Figure 6: Lir decreases pro-atherogenic cell populations *in vivo*

A| Bone marrow monocytes, B| BMDMs, C| ratio of bone marrow monocytes to BMDMs, D| splenic macrophages and E| LNs were analyzed by flow cytometry. Cells from bone marrow, spleen and LNs were analyzed according to the antibodies listed in Table 1. Error bars are representative of A-E| n=5. Statistical analysis was performed carrying out Mann Whitney tests between LFD vs HFHCD where statistical significance was considered with *$p<0.05$, **$p<0.01$ and ***$p<0.001$ and HFHCD vs HFHCD+Lir where $^{\$}p<0.05$, $^{\$\$}p<0.01$ and $^{\$\$\$}p<0.001$ were considered significant.

JPET Fast Forward. Published on July 3, 2019 as DOI: 10.1124/jpet.119.258343
This article has not been copyedited and formatted. The final version may differ from this version.

Table 1: Flow cytometry antibodies

Antibodies used for flow cytometry analysis of bone marrow cells, spleens and LNs.

Cell	***Antibodies***
Inflammatory bone marrow monocytes	$CD45^{+}$ $CD115^{+}$ $F4/80^{+}$ $Ly6C^{+}$ $CD11c^{-}$
Resident bone marrow monocytes	$CD45^{+}$ $CD115^{+}$ $F4/80^{+}$ $Ly6C^{-}$ $CD11c^{+}$
M1-like BMDMs	$CD45^{+}$ $CD115^{+}$ $CD11b^{+}$ $F4/80^{+}$ $Ly6C^{hi}$
M2-like BMDMs	$CD45^{+}$ $CD115^{+}$ $CD11b^{+}$ $F4/80^{+}$ $Ly\text{-}6C^{lo}$
Monocytes and DCs in LNs	$CD45^{+}$ $CD11b^{int}$ $Ly6C^{int}$ $F4/80^{lo}$ $CD11c^{int}$
DCs in LNs	$CD45^{+}$ $CD11b^{lo}$ $Ly6C^{lo}$ $F4/80^{lo}$ $CD11b^{hi}$
Splenic M1 macrophages	$CD45^{+}$ $CD11b^{hi}$ $F4/80^{hi}$ $CD11c^{lo}$ $Ly6C^{hi}$
Splenic M2 macrophages	$CD45^{+}$ $CD11b^{hi}$ $F4/80^{hi}$ $CD11c^{lo}$ $Ly6C^{lo}$

Table 2: SYBR® Green primer sequences

SYBR® Green Primer	***Gene Sequence***
Human TNF-α forward	5'-CTCGAACCCCGAGTGACAA-3'
Human TNF-α reverse	5'-GCTGCCCCTCAGCTTGAG-3'
Murine iNOS forward	5'-CCCTCCTGATCTTGTGTTGGA-3'
Murine iNOS reverse	5'-CCACCCGAGCTCCTGGAAC-3'
Murine TNF-α forward	5'-GGCAGGTCTACTTTGGAGTCATTGC-3'
Murine TNF-α reverse	5'-ACATTCGAGGCTCCAGTGAATTCGG-3'

JPET Fast Forward. Published on July 3, 2019 as DOI: 10.1124/jpet.119.258343
This article has not been copyedited and formatted. The final version may differ from this version.

Figure 1

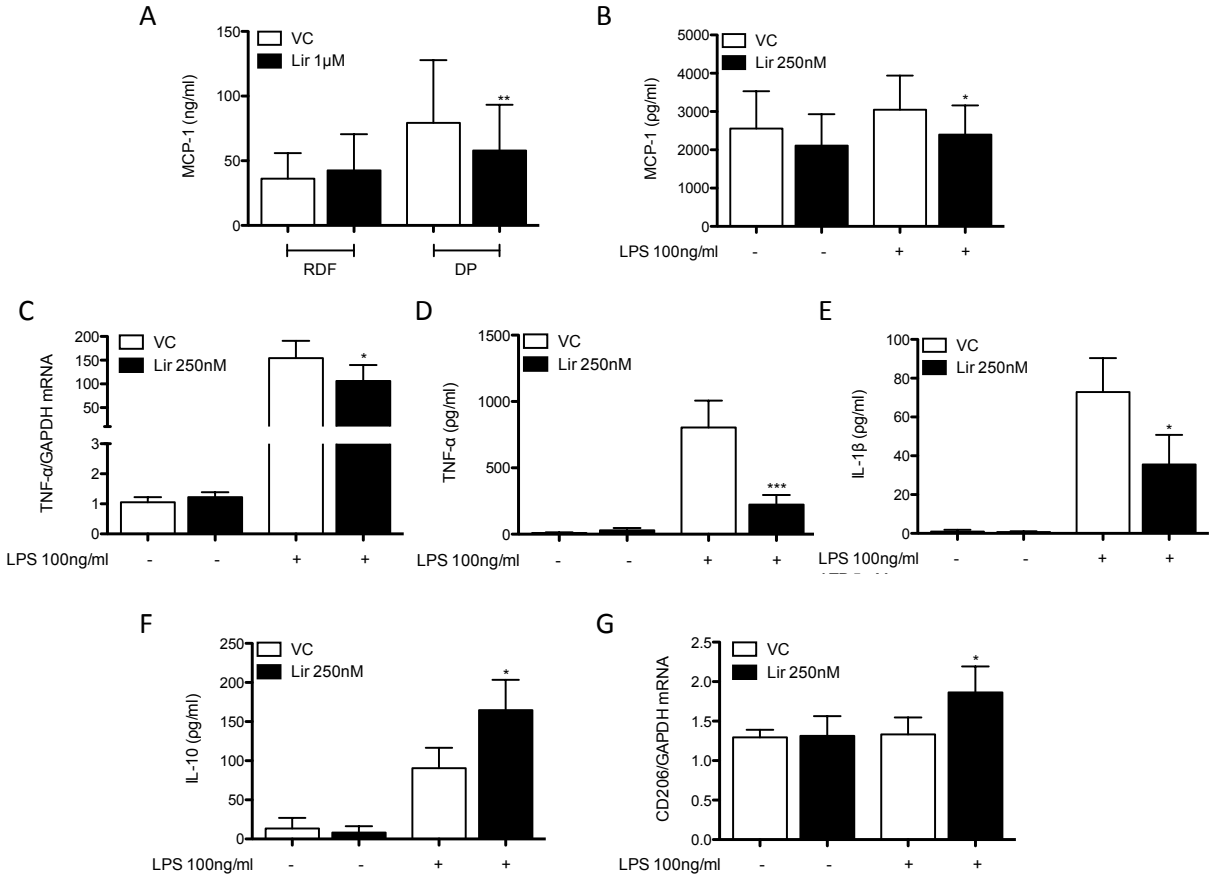

JPET Fast Forward. Published on July 3, 2019 as DOI: 10.1124/jpet.119.258343
This article has not been copyedited and formatted. The final version may differ from this version.

Figure 2

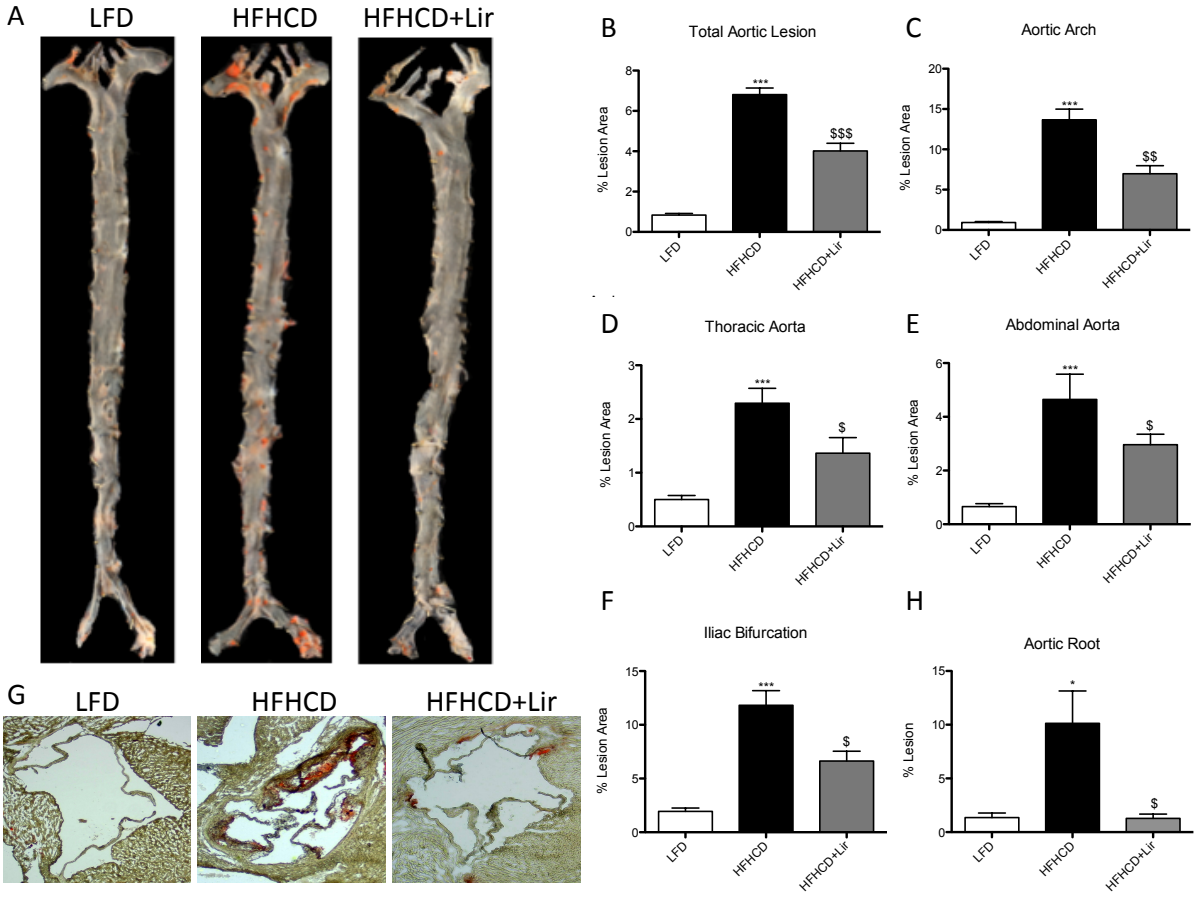

JPET Fast Forward. Published on July 3, 2019 as DOI: 10.1124/jpet.119.258343
This article has not been copyedited and formatted. The final version may differ from this version.

Figure 3

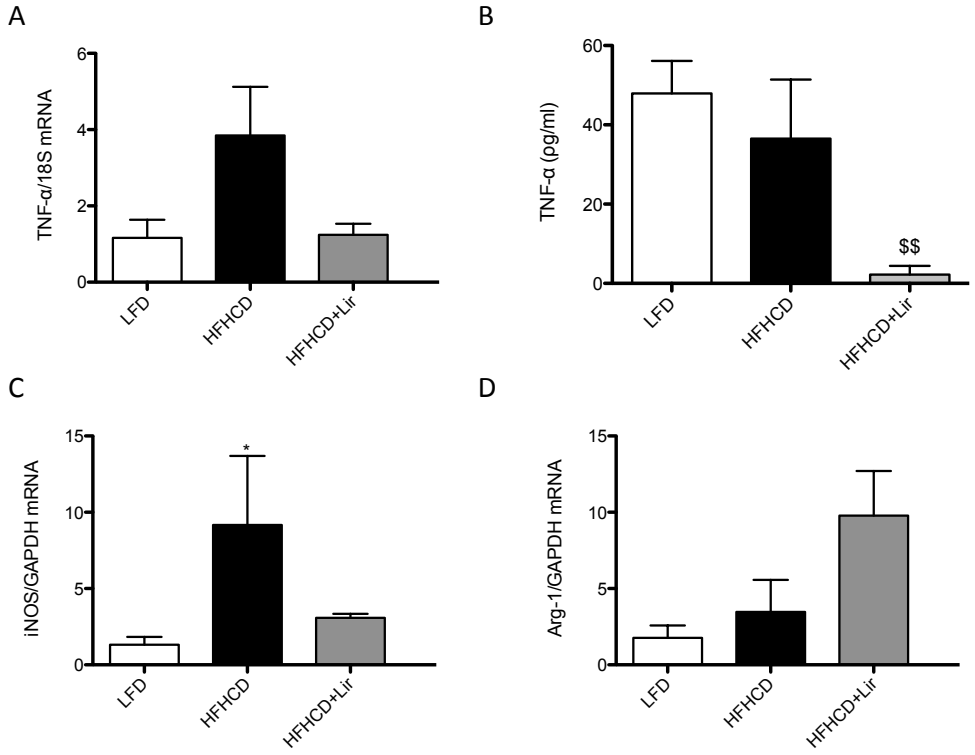

JPET Fast Forward. Published on July 3, 2019 as DOI: 10.1124/jpet.119.258343
This article has not been copyedited and formatted. The final version may differ from this version.

Figure 4

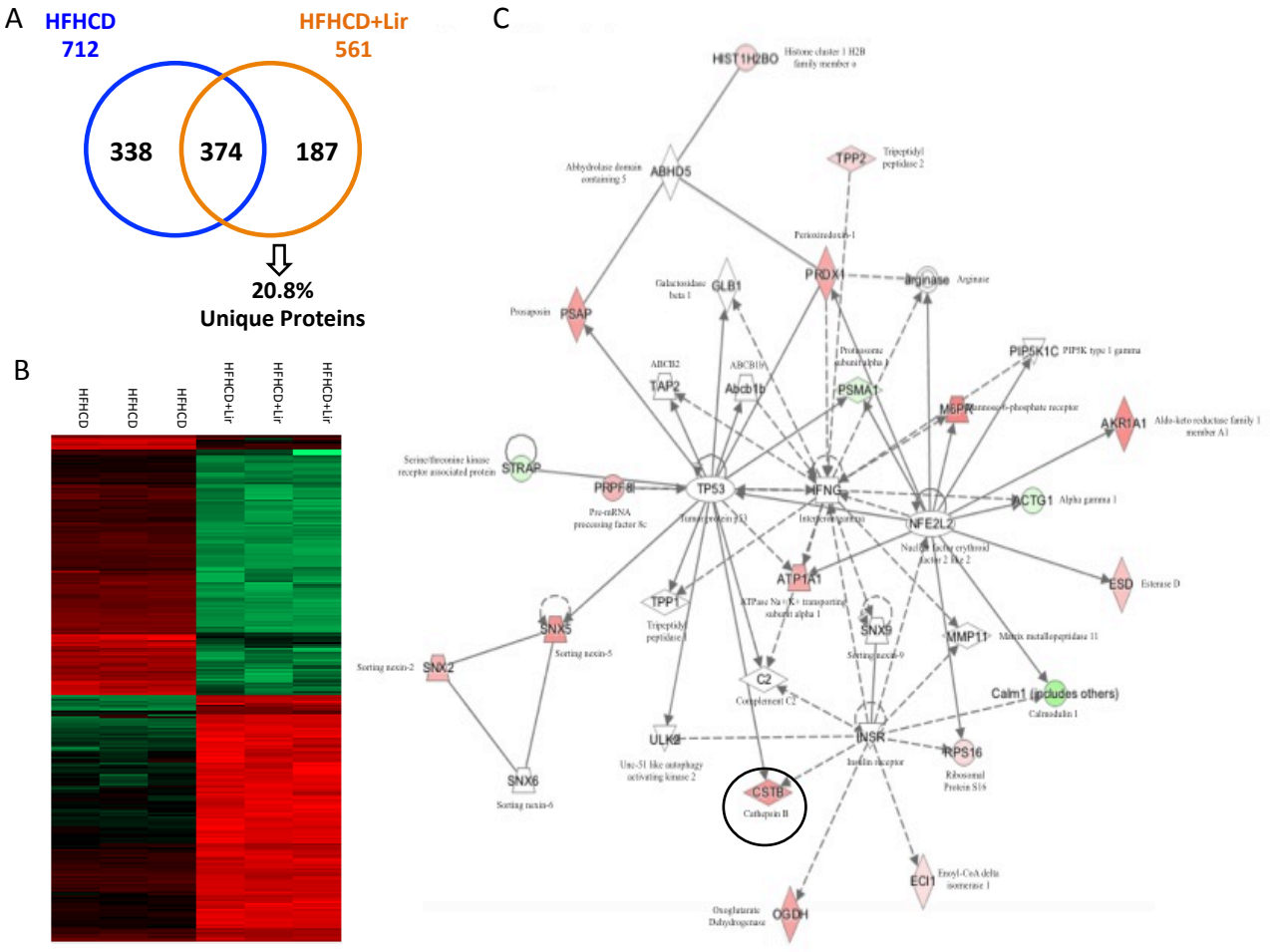

JPET Fast Forward. Published on July 3, 2019 as DOI: 10.1124/jpet.119.258343
This article has not been copyedited and formatted. The final version may differ from this version.

Figure 5

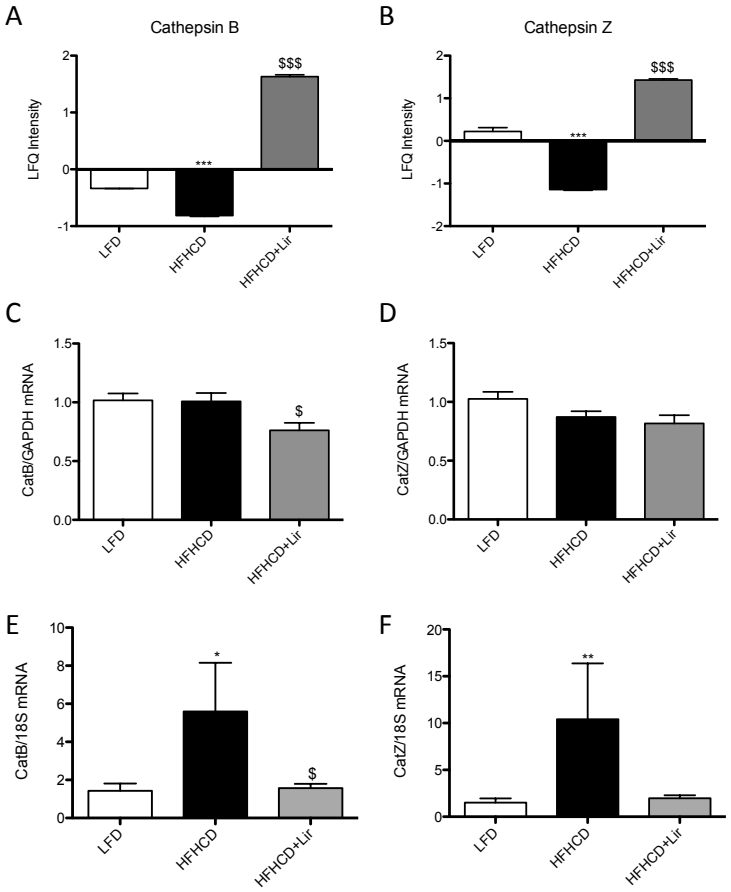

JPET Fast Forward. Published on July 3, 2019 as DOI: 10.1124/jpet.119.258343
This article has not been copyedited and formatted. The final version may differ from this version.

Figure 6

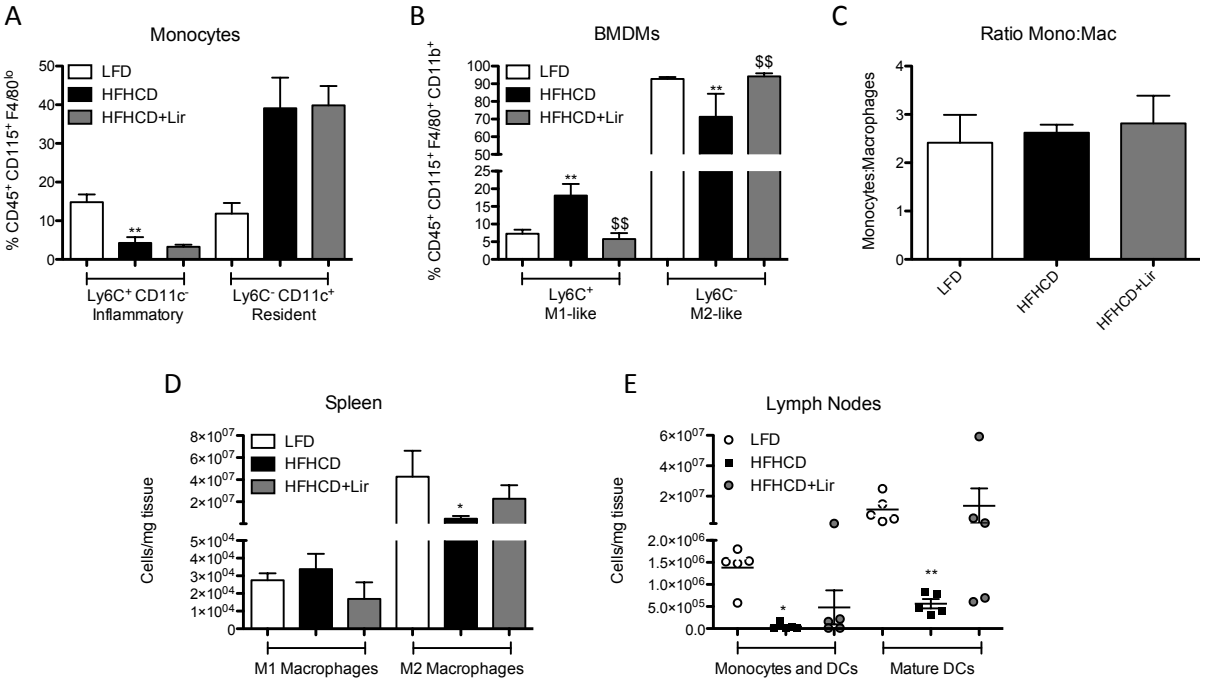

Article Title: Liraglutide attenuates pre-established atherosclerosis in apolipoprotein E deficient mice *via* regulation of immune cell phenotypes and pro-inflammatory mediators

Authors: Robyn Bruen[1], Seán Curley[2] Sarina Kajani[2], Gina Lynch[3], Marcella E. O'Reilly[3], Eugène T. Dillon[4], Eoin P. Brennan[2], Mary Barry[5], Stephen Sheehan[5] Fiona C. McGillicuddy[2] and Orina Belton[1*].

Journal Title: The Journal of Pharmacology and Experimental Therapeutics

Supplementary Methods

Immunohistochemistry

Frozen aortic root slides were fixed in acetone (-20 ^{o}C) for 10min, air-dried for 20min and submerged in tris buffered saline solution prior to immunohistochemical staining. The endogeneous peroxidase activity and non-specific staining was blocked with 30% hydrogen peroxide, non-serum protein block (Agilent Dako X0909) and T20 blocking buffer (ThermoFisher 37543). Without rinising the later the rat anti-F4/80 antibody (1:500, Abcam ab6640) was applied and incubated for 30min. The tissue sections were then incubated with an anti-rat secondary antibody (1:500, Agilent Dako P0450) for 20min. A rabbit-HRP enhancer (Enzo, ENZ-ACC110) was applied for 20min before addition of 3,3'-diaminobenzidine for 5min revelation. The slides were counterstained with haematoxylin and rinsed in dH_2O. Positive and negative control tissue was stained for F4/80. The negative control slide was run under identical conditions in the absence of primary antibody. Murine frozen spleen sections were used as positive control tissue. The slides were dried in an oven (58 ^{o}C) and permanently mounted. Once dry the slides were digitized using the Leica Aperio AT2 digital slide scanner. The subsequent images were analysed using the Aperio

Cytoplasmic v2 Algorithim, which has been trained to recognize and quantify F4/80 cells in the aortic root areas of heart sections.

Supplemental Tables

Target antigen	Catalog #	Working concentration	Lot #
CD45-BB515 Clone 30-F11	564590	4µg/ml	6021897
CD115-PE Clone T38-320	565249	6µg/ml	6050996
CD11c-PE-Cy7 Clone HL3	558079	8µg/ml	5176789
Ly6C-APC Clone AL-21	560595	2µg/ml	5321849
F4/80 Clone T45-2342	565411	4µg/ml	6091779
CD11b-BV510 Clone M1/70	562950	4µg/ml	5306509

Supplemental Table 1: Antibodies for flow cytometry

Protein Name	**Protein ID**	**Uniprot ID**	**Expression**
Small ubiquitin-related modifier 1	SUMO1	P63166	Down
Cathepsin Z	CATZ	Q9WUU7	Up
Cathepsin B	CATB	P10605	Up
Sorting nexin-2	SNX2	Q9CWK8	Up
Lysosome-associated membrane glycoprotein 1	LAMP1	P11438	Up
Annexin A4	ANXA4	P97429	Up
Far upstream element-binding protein 2	FUBP2	Q3U0V1	Down
Rho GDP-dissociation inhibitor 2	GDIR2	Q61599	Down
RNA-binding protein 3	RBM3	O89086	Down
Flavin reductase (NADPH)	BLVRB	Q923D2	Down
Transmembrane emp24 domain-containing protein 10	TMEDA	Q9D1D4	Up
Lamin-B2	LMNB2	P21619	Down
Cytoskeleton-associated protein 4	CKAP4	Q8BMK4	Down
Elongation factor 1-delta	Q80T06	Q80T06	Down
Prelamin-A/C	LMNA	P48678	Up
Lamin-B1	LMNB1	P14733	Down
Isoform 2 of Protein SET	SET	Q9EQU5-2	Down

Clathrin heavy chain 1	CLH1	Q68FD5	Up
Plasminogen activator inhibitor 1 RNA-binding protein	PAIRB	Q9CY58	Down
Voltage-dependent anion-selective channel protein 1	VDAC1	Q60932-2	Up
Endoplasmin	ENPL	P08113	Up
Cathepsin D	F8WIR1	F8WIR1	Up
Dihydropyrimidinase-related protein 2	DPYL2	O08553	Up
Transforming protein RhoA	RHOA	Q9QUI0	Up
Elongation factor 2	EF2	P58252	Up

Supplemental Table 2: Top 25 significant proteins (*p<0.05) HFHCD+Lir vs HFHCD

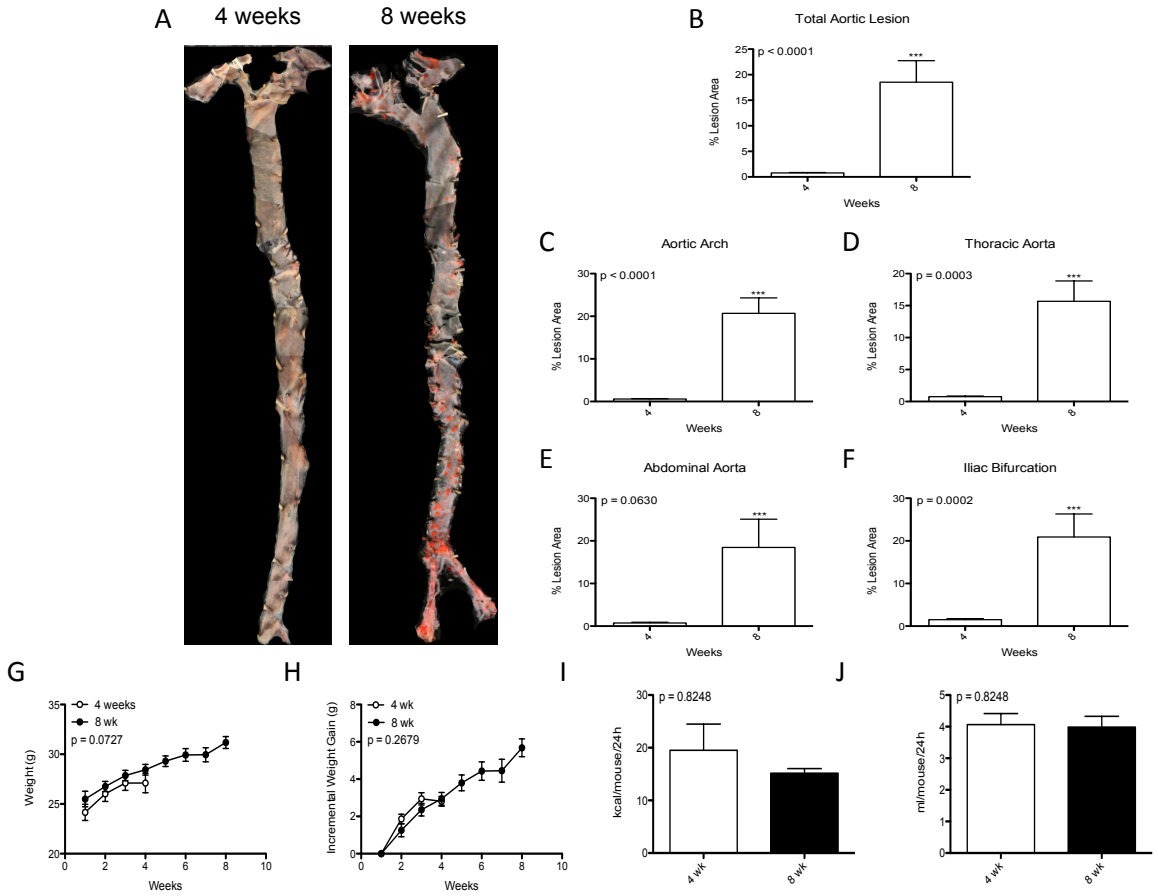

Supplemental Figure 1: HFHCD feeding increases lesion development in ApoE$^{-/-}$ mice

ApoE$^{-/-}$ mice were fed a HFHCD for 4 or 8wks. A| *En face* Sudan IV staining was performed on aortae and %lesion areas were quantified for B| total aorta, C| aortic arch, D| thoracic aorta, E| abdominal aorta and F| iliac bifurcation using ImageJ. G| Weights of mice in grams was graphed and H| incremental weight change was calculated in grams. I| Calorie (kcal) intake and J| water intake (ml) per cage was measured weekly throughout the study. Graphs were constructed using GraphPad Prism 5. Error bars are representative of A-J| 10 aortae or mice per group (n=10). Statistical analysis was carried out performing Mann-Whitney t-tests for each group, with ***$p<0.001$ and $p>0.05$ was considered ns.

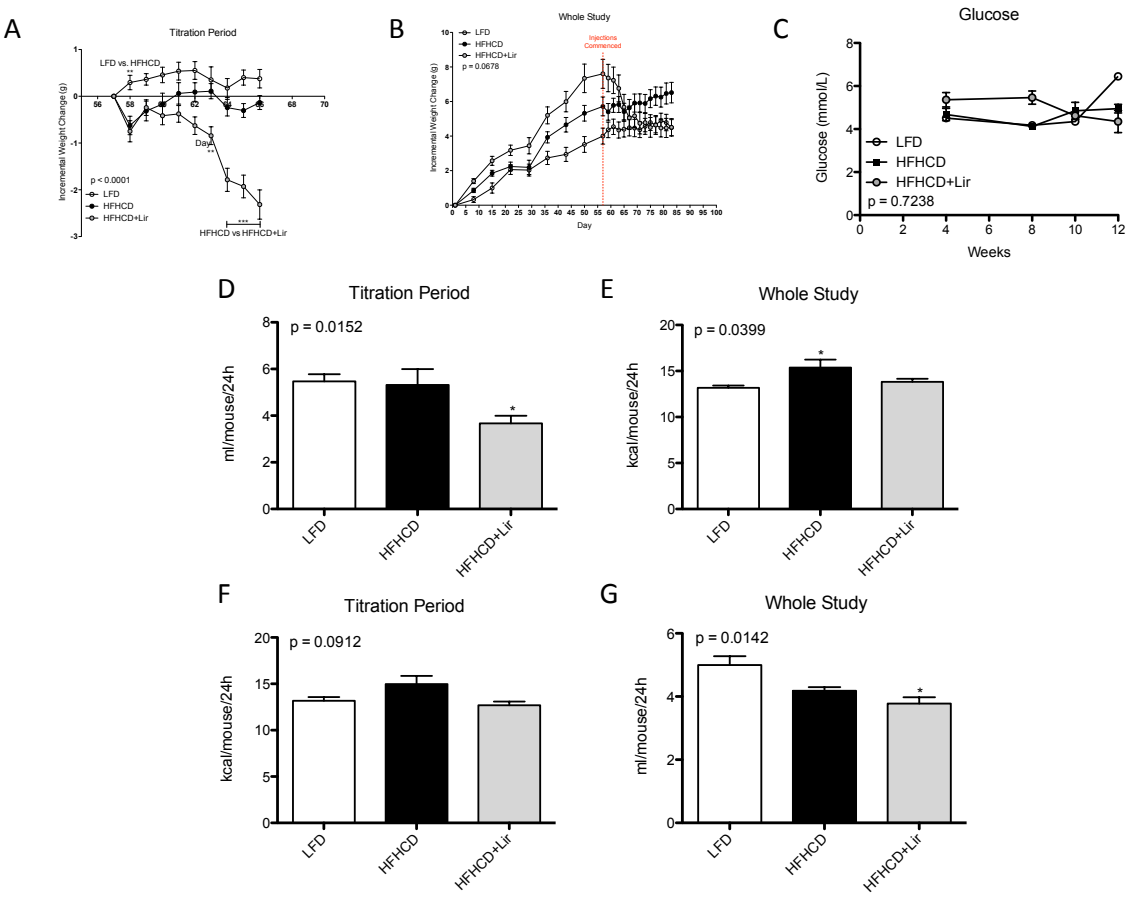

Supplemental Figure 2: ApoE$^{-/-}$ mice body weight, food, glucose, calorie and water intake

ApoE$^{-/-}$ mice were fed a LFD or HFHCD wks 1-12 and wks 9-12 mice received daily s.c. injections of 300µg/kg Lir or VC PBS. Mice were weighed weekly 1-8wk and daily 9-12wk. Incremental weight change was calculated for A| titration dose period and B| whole study. C| Fasting blood glucose was measured bi-weekly from wks 4-12. Food intake per cage was measured weekly for D| the titration dose period and E| whole study. Water intake per cage was measured weekly wks 1-8 and daily wks 9-12 for F| the titration dose period and G| whole study. Error bars are representative of A-B| twenty-one mice per group (n=21), C| four to eight mice (n=4-8), D-G| seven cages (n=7). Statistical analysis was performed with Kruskal-Wallis tests followed by Dunn's multiple comparison post-test. Statistical significance was considered when *$p<0.05$ and $p>0.05$ was ns, with stars above the columns represent comparisons against the LFD control.

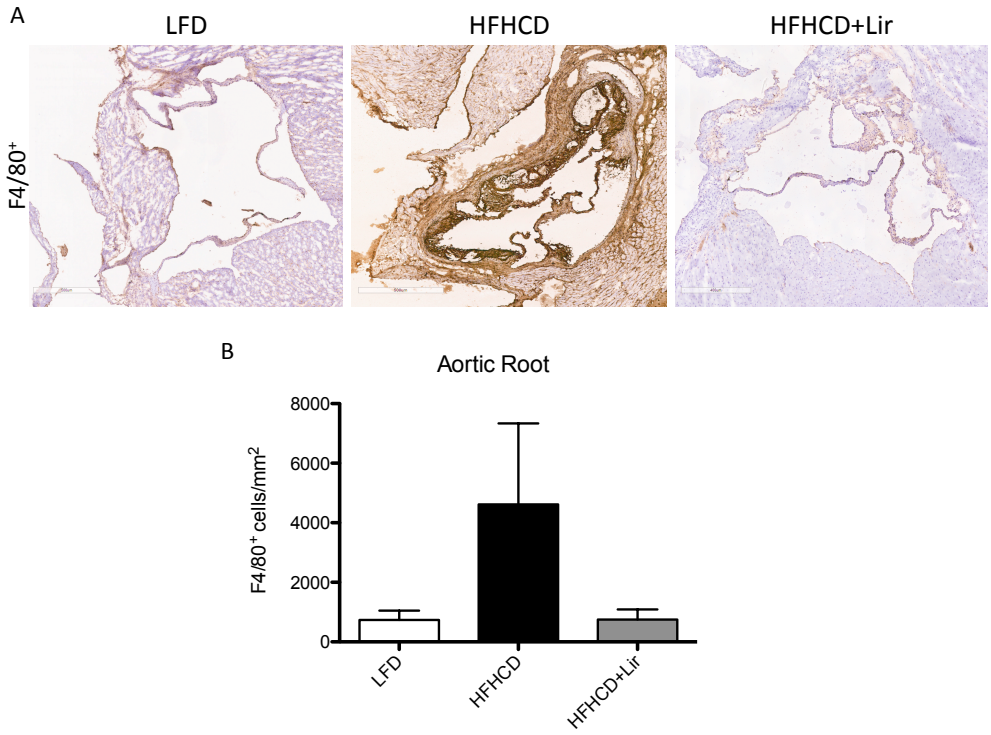

Supplemental Figure 3: Aortic root staining for F4/80+ macrophages

Hearts of ApoE$^{-/-}$ mice treated with LFD 12wks, a HFHCD 8wks followed by either daily s.c. Lir or VC injections for a further 4wks (total 12wks) were cryosectioned for the aortic root and stained for F4/80 by immunohistochemistry. A| Positive cells for F4/80 staining are indicated by the brown colour. B| The number of F4/80^{+} cells/mm^{2} of aortic root tissue were quantified and graphed using GraphPad Prism 5.0c. Statistical analysis was performed carrying out a Mann Whitney tests comparing LFD vs HFHCD and HFHCD vs HFHCD+Lir. Statistical significance was considered when $p<0.05$ and NS when $p>0.05$.

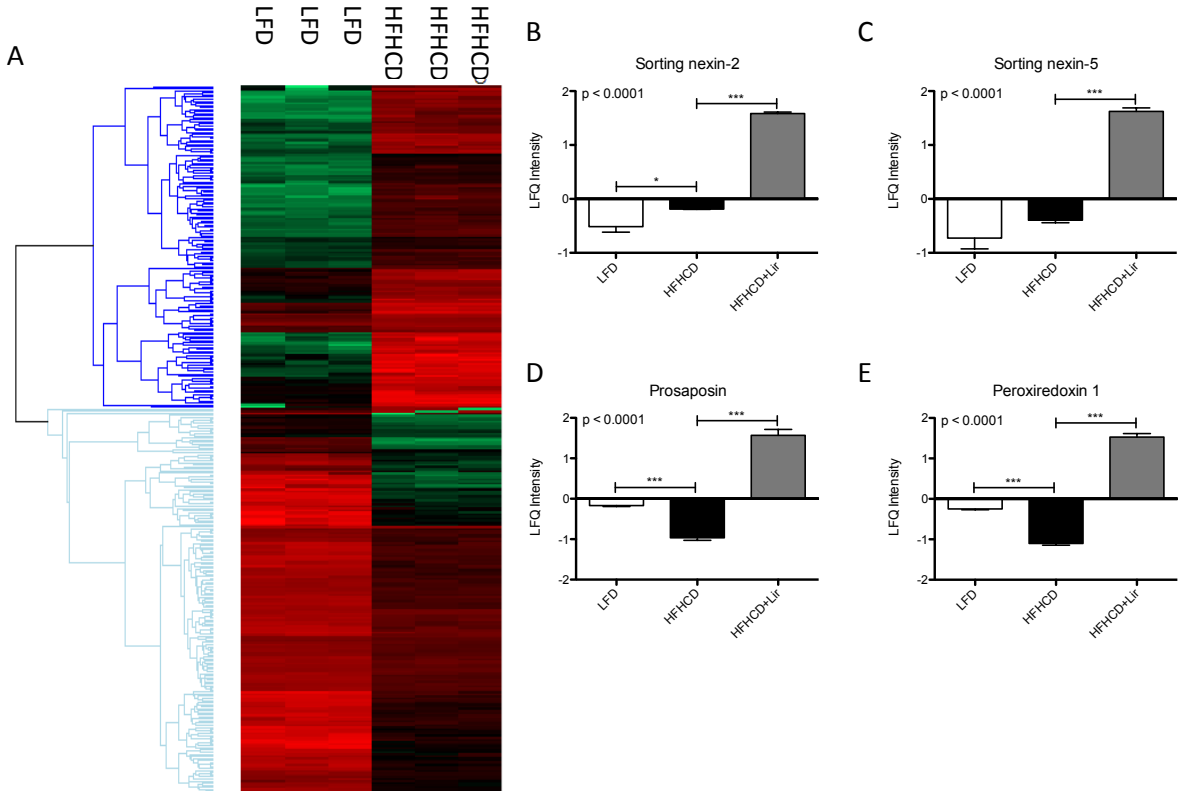

Supplemental Figure 4: Proteomic signature of LFD vs HFHCD and proteins altered from HFHCD+Lir network

Bone marrow cells were subjected to proteomic analysis where A| LFD vs HFHCD signature is displayed. Up-regulated proteins altered in HFHCD+Lir compared to HFHCD control from the inflammatory network show B| sorting nexin-2, C| sorting nexin-5, D| prosaposin and E| peroxiredoxin (PRDX)-1. An unpaired t-test was carried out comparing groups and ***$p<0.01$ was considered statistically significant, where capped lines indicate comparisons made between groups.